

Temperature, brightness and spectral index of the Cygnus radio loop

V. Borka Jovanović^{1,*} and D. Urošević²

¹*Atomic Physics Laboratory (040), Vinča Institute of Nuclear Sciences,
University of Belgrade, P.O. Box 522, 11001 Belgrade, Serbia*

²*Department of Astronomy, Faculty of Mathematics,
University of Belgrade, Studentski trg 16, 11000 Belgrade, Serbia*

(Dated: March 11, 2011)

The estimated brightness of the Cygnus loop supernova remnant (SNR) at 2720, 1420, 820, 408 and 34.5 MHz are presented. The observations of the continuum radio emission are used to calculate the mean brightness temperatures and surface brightnesses of this loop at the five frequencies in wide spectral range, using the method we have previously developed for large radio loops. The spectrum for mean temperatures versus frequency between the five frequencies is estimated and the spectral index of Cygnus loop is also obtained. Also, from our results can be concluded that Cygnus loop evolves in the low density environment and the initial energy of supernova explosion was relatively low. The obtained results confirm non-thermal origin of the Cygnus radio loop and show that our method is applicable to almost all remnants.

PACS numbers: 12.39.Jh, 12.40.Yx, 14.65.Bt, 14.65.Dw

Keywords: surveys; radio continuum: general; ISM: supernova remnants; radiation mechanisms: non-thermal.

I. INTRODUCTION

In our investigation, we are supposing the radio loops to be evolved supernova remnants (SNRs). Supernova remnants represent shells of approximately spherical shape which are spreading, and depending of the interstellar matter density, they change their shape. We can see only parts of these spherical contours which represent radio spurs, e.g. areas of more intense emission in the sky, spur-like and of huge dimensions. Radio loops consist of more spurs lying approximately in the same small circle of the celestial sphere. Their material probably expands inside of bubbles of low density. Bubbles are made by former SNR explosions or by strong stellar winds (McKee & Ostriker [1], Salter [2] and references therein). The radio emission from SNRs is generally understood to be synchrotron emission from the relativistic electrons moving in the magnetic field.

A star in the constellation of Cygnus exploded and its remnant is Cygnus loop. It is classified as a middle-aged SNR of type S, located below (but near the plane of) the Galactic equator, and less than 1 kpc away from us. It is listed in Green's catalogue of SNRs as G74.0-8.5 (Green [3, 4, 5]). As shown in Green [6], this remnant has been decelerated considerably by its interaction with the surrounding interstellar medium.

Leahy, Roger, & Ballantyne [7] presented high resolution 1420 MHz total intensity and polarization maps of the Cygnus loop and derived rotation measures. Aschenbach & Leahy [8] made a comparison between the radio and X-ray emission from supernova remnants. The X-ray emission traces the hot gas behind the shock front, while

the radio emission comes from the relativistic electron population emitting synchrotron radiation in the ambient magnetic field. They found that there are significant differences in the distribution of X-ray and radio brightness in the Cygnus loop. Also, significant temperature variations, seen along the rim and in the bright filaments interior to the rim, pointed out that the Cygnus loop was caused by a supernova exploding in a cavity.

Uyaniker et al. [9] suggested that Cygnus loop may consist of two overlapping remnants. Substantial differences between the northern and southern part as well as in their emission characteristics have been observed (Pataude et al. [10], Uyaniker et al. [11]). Some authors proposed that the Cygnus loop consists of two likely interacting SNRs: G74.3-8.4 and G72.9-9.0 (Uyaniker et al. [9], Leahy [12]). In Sun et al. [13], from 4800 MHz observations, it is explained that the polarization maps (the difference in the polarization characteristic between the northern and southern part) support previous ideas that the Cygnus loop may consist of two SNRs. Besides, several compact radio sources are located within the boundary of the remnant. The main characteristics of the Cygnus loop in different spectral bands are: (a) in radio band: it is shell, brightest to the north-east, with fainter breakout region to south, with spectral variations, (b) optical: large filamentary loop, brightest to the north-east, not well defined to the south and west, (c) X-ray: shell in soft X-rays (see e.g. in Green [4]).

Some radio maps which include this remnant are the following: the map by Kundu & Becker [14] at 4940 MHz, Keen et al. [15] at 2695 MHz, Uyaniker et al. [11] at 2675 MHz, Leahy, Roger, & Ballantyne [7] at 1420 MHz, Dickel & Willis [16] at 610 MHz, Green [6] at 408 MHz. Observations of the continuum radio emission at 2720 (Reif et al. [17]), 1420 (Reich & Reich [18]), 820 (Berkhuijsen [19]), 408 (Haslam et al. [20]) and 34.5 MHz (Dwarakanath & Udaya Shankar [21]), we found in

*Corresponding author: vborka@vinca.rs

electronic form and used them in this paper.

In our previous paper (Borka Jovanović & Urošević [22]) we only calculated the temperatures and brightnesses at the three frequencies. In this paper we expand the scope of our investigation to: brightness temperatures and surface brightnesses at the five frequencies, as well as spectrum, $T-T$ graphs, the radio spectral indices, estimation of environment density and the initial energy of supernova explosion, and the flux density spectrum.

In our calculations, we used brightness temperatures over the whole area of the loop, so the mean temperature that we estimated refers to northern and southern parts together. In this research the average brightness temperatures and surface brightnesses of the Cygnus radio loop are calculated at the five frequencies: 2720, 1420, 820, 408 and 34.5 MHz. Then we study how these results are getting along with previous results (Uyaniker et al. [11], Reich, Zhang & Fürst [23], Roger et al. [24]) and with current theories of SNR evolution. These theories predict that loops are non-thermal sources which are spreading inside of the hot and low density bubbles made by former supernova explosions or by strong stellar winds (see McKee & Ostriker [1], Salter [2] and references therein).

Our aim is also to apply method for determination of the brightness temperature given in article Borka [25] which is developed for large radio loops, and to show that it is rather efficient in the case of much smaller radio loops, e.g. Cygnus loop, as well as to check how the results obtained using this method are getting along with the method of $T-T$ graphics and results obtained with other methods. Our method is quite simple because we are using brightness temperature isolines to define borders of the Cygnus loop at the wide range of frequencies ($\nu_{max}/\nu_{min} = 2720 \text{ MHz} / 34.5 \text{ MHz} \approx 79$). Other authors are using different squared or rectangular areas to determine area of the loop and calculate spectral indices, brightness temperature and the flux of the loop (Uyaniker et al. [11], page 917 and Leahy & Roger [26], page 786). Also, we calculated flux from Cygnus loop and compare our results with results of other authors in different frequency ranges.

II. ANALYSIS

Data

We used the following radio-continuum surveys as the basic source of data in this paper: at 2720 MHz (Reif et al. [17]), 1420 MHz (Reich & Reich [18]), 820 MHz (Berkhuijsen [19]), 408 MHz (Haslam et al. [20]) and 34.5 MHz (Dwarakanath & Udaya Shankar [21]). These surveys are available in electronic form, as the "Flexible Image Transport System" (FITS) data format, at the site: <http://www.mpifr-bonn.mpg.de/survey.html>. This online Survey Sampler of the "Max-Planck-Institut für Radioastronomie" (MPIfR) near Bonn, Germany, al-

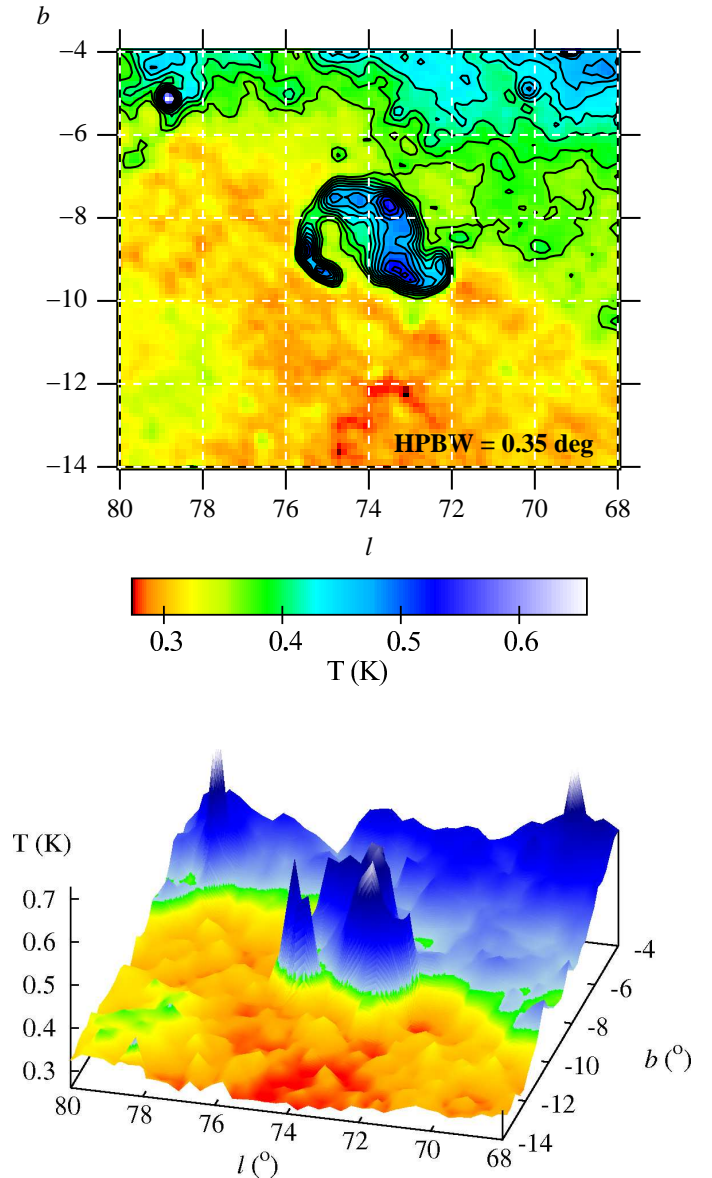


FIG. 1: *Top*: the 2720 MHz map of a region in Cygnus, in new Galactic coordinates (l, b) , showing contours of brightness temperature. This radio loop has position: $l = [76.5^\circ, 71.5^\circ]$; $b = [-10.5^\circ, -7^\circ]$. The HPBW (Half Power Beam Width) for this frequency is $0^\circ.35$. Eleven contours plotted represent the temperatures T_{min} and T_{max} from Table I and nine contours in between. The contours are plotted every 0.265 K, starting from the lowest temperature of 0.395 K up to 0.66 K. The corresponding temperature scale is given (in K). *Bottom*: the 2720 MHz area map of Cygnus.

lows users to pick a region of the sky and obtain images and data at different frequencies. The 2720-MHz Stockert survey has the angular resolution of $0^\circ.35$, 1420-MHz Stockert survey (Reich & Reich [18]) $0^\circ.59$, the 820-MHz Dwingeloo survey (Berkhuijsen [19]) $1^\circ.2$, the 408-MHz all-sky survey (Haslam et al. [20]) $0^\circ.85$ and the 34.5-MHz Gauribidanur survey (Dwarakanath & Udaya Shankar [21]) $0^\circ.7$. The corresponding observations are

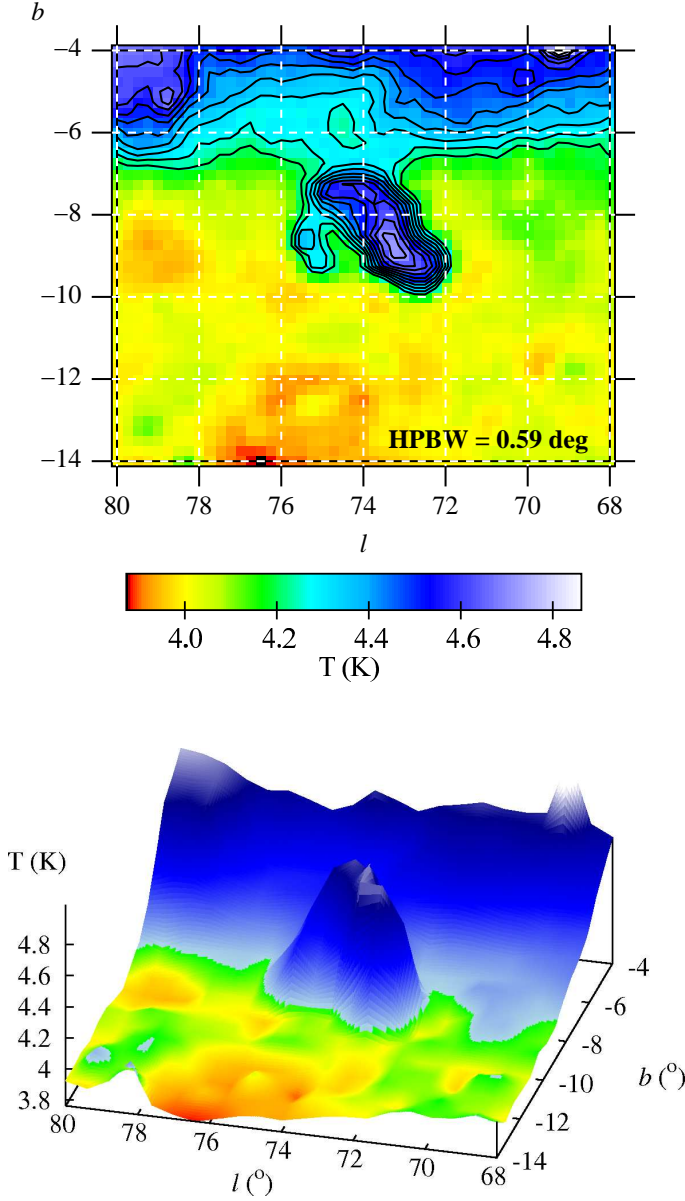


FIG. 2: The same as Fig. 1, but for 1420 MHz. The HPBW for this frequency is $0^{\circ}.59$. The contours are plotted every 0.07 K, starting from the lowest temperature of 4.2 K up to 4.9 K.

given at the following rates (measured data) for both l and b : $\frac{1^{\circ}}{8}$ at 2720 MHz, $\frac{1^{\circ}}{4}$ at 1420 MHz, $\frac{1^{\circ}}{2}$ at 820 MHz, $\frac{1^{\circ}}{3}$ at 408 MHz and $\frac{1^{\circ}}{5}$ at 34.5 MHz. The effective sensitivities are about 5 mK T_b (T_b is for an average brightness temperature), 50 mK, 0.20 K, 1.0 K and about 700 K, respectively.

FITS data format stores the multidimensional arrays and 2-dimensional tables containing rows and columns of scientific data sets. We extracted observed brightness temperatures from this data format into ASCII data files, and afterwards using our programs in C and FORTRAN, we obtained results presented in this paper.

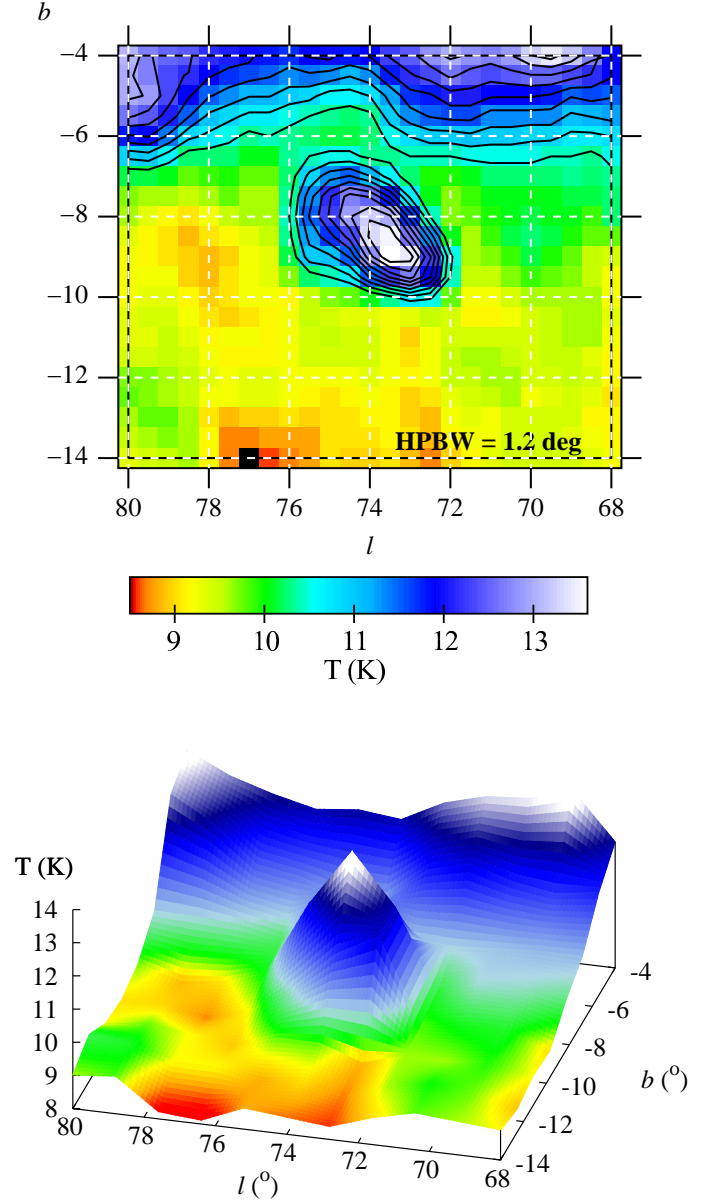


FIG. 3: The same as Fig. 1, but for 820 MHz. The HPBW is $1^{\circ}.2$. The contours are plotted every 0.39 K, starting from the lowest temperature of 10.1 K up to 14 K.

Method

As there is great influence of background radiation over the Cygnus loop area, it is very difficult to determine its area precisely. The area of this loop is enclosed with brightness temperature contours. The maps of a region in Cygnus, in new Galactic coordinates (l , b), with contours of the brightness temperatures T_b are plotted in Figs. 1–5. In these figures, among all the brightness temperature contours, the most important are the outer contour and inner one which represent the loop borders. The outer one (which corresponds to the minimum temperature of the loop) separates loop and background, while the inner

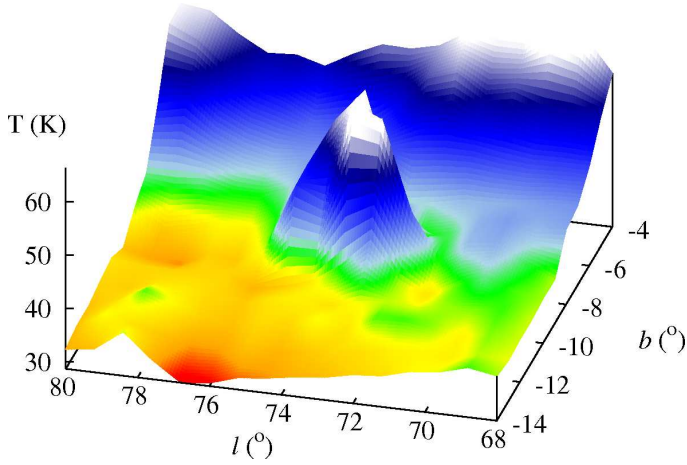
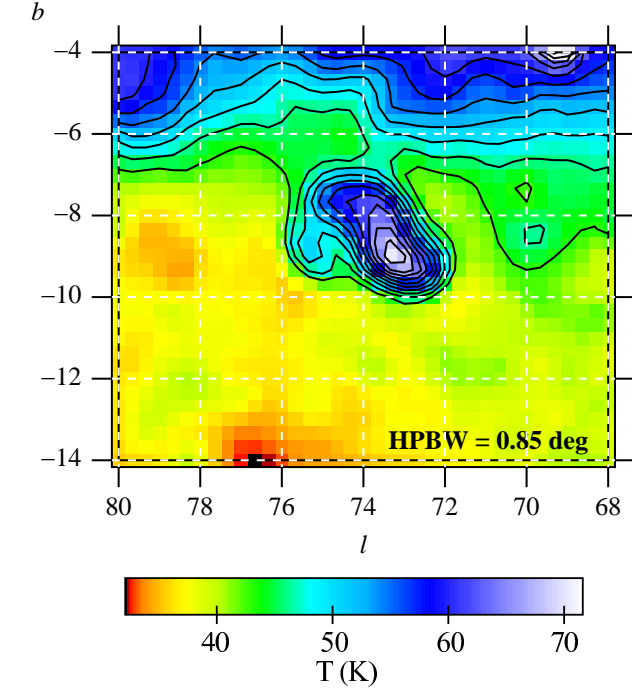


FIG. 4: The same as Fig. 1, but for 408 MHz. The HPBW is $0^\circ.85$. The contours are plotted every 3.1 K, starting from the lowest temperature of 41 K up to 72 K.

one (corresponding to the maximum temperature) separates loop and some superposed source. The interval of Galactic longitude of this loop is $l = [76.5^\circ, 71.5^\circ]$, and of latitude is $b = [-10.5^\circ, -7^\circ]$. We used the same method of calculation as given in Borka [25] for Galactic radio loops I–VI, Borka, Milogradov-Turin, & Urošević [27] for Loops V and VI and in Borka Jovanović & Urošević [28] for Monoceros loop. Our aim is to apply method, which we developed for main Galactic loops I–VI and described in Borka [25] and Borka, Milogradov-Turin, & Urošević [27], to smaller remnants and to show that our method of calculation is applicable to almost all remnants. To confirm that our method is good, we also gave

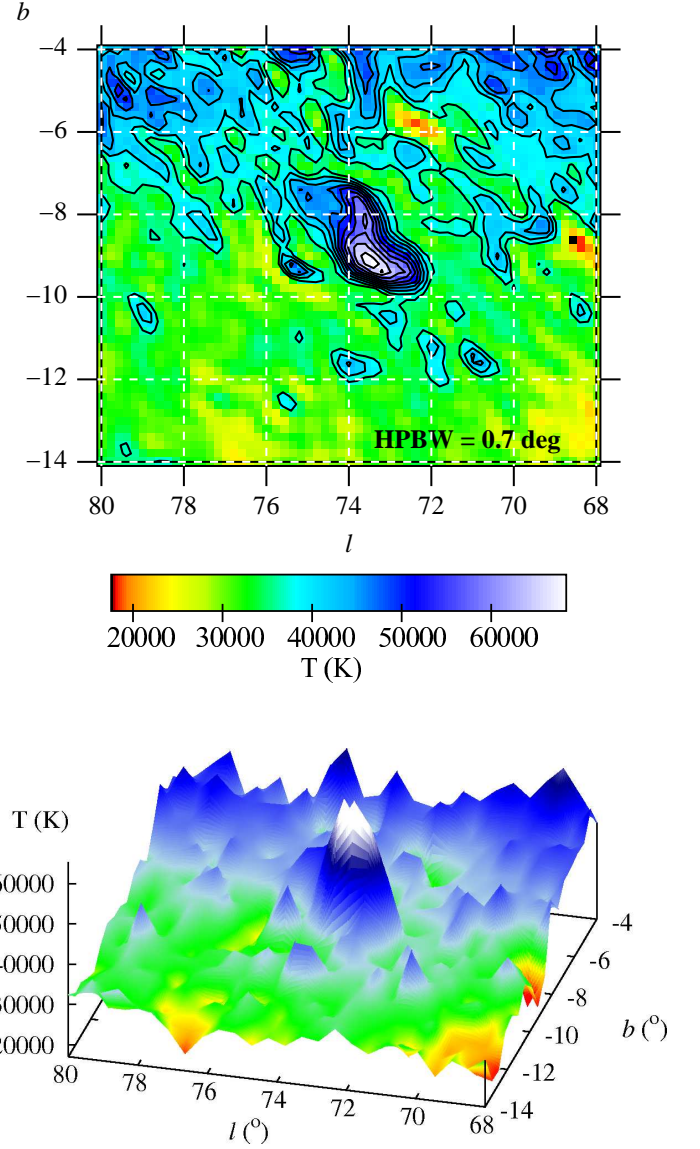


FIG. 5: The same as Fig. 1, but for 34.5 MHz. The HPBW is $0^\circ.7$. The contours are plotted every 3550 K, starting from the lowest temperature of 34500 K up to 70000 K.

the area maps of Cygnus at the five frequencies (Figs. 1–5) and some examples of the temperature profiles at the 2720 MHz (Fig. 6). In Fig. 6 it should be noticed that the bottom panel shows only background radiation (not including loop), where for $b = -10^\circ$ the brightness temperature is not higher than 0.38 K. It is in agreement with temperature intervals given in the first row of the Table I, where for the minimum temperature of the loop with background, at 2720 MHz, it is put 0.395 K.

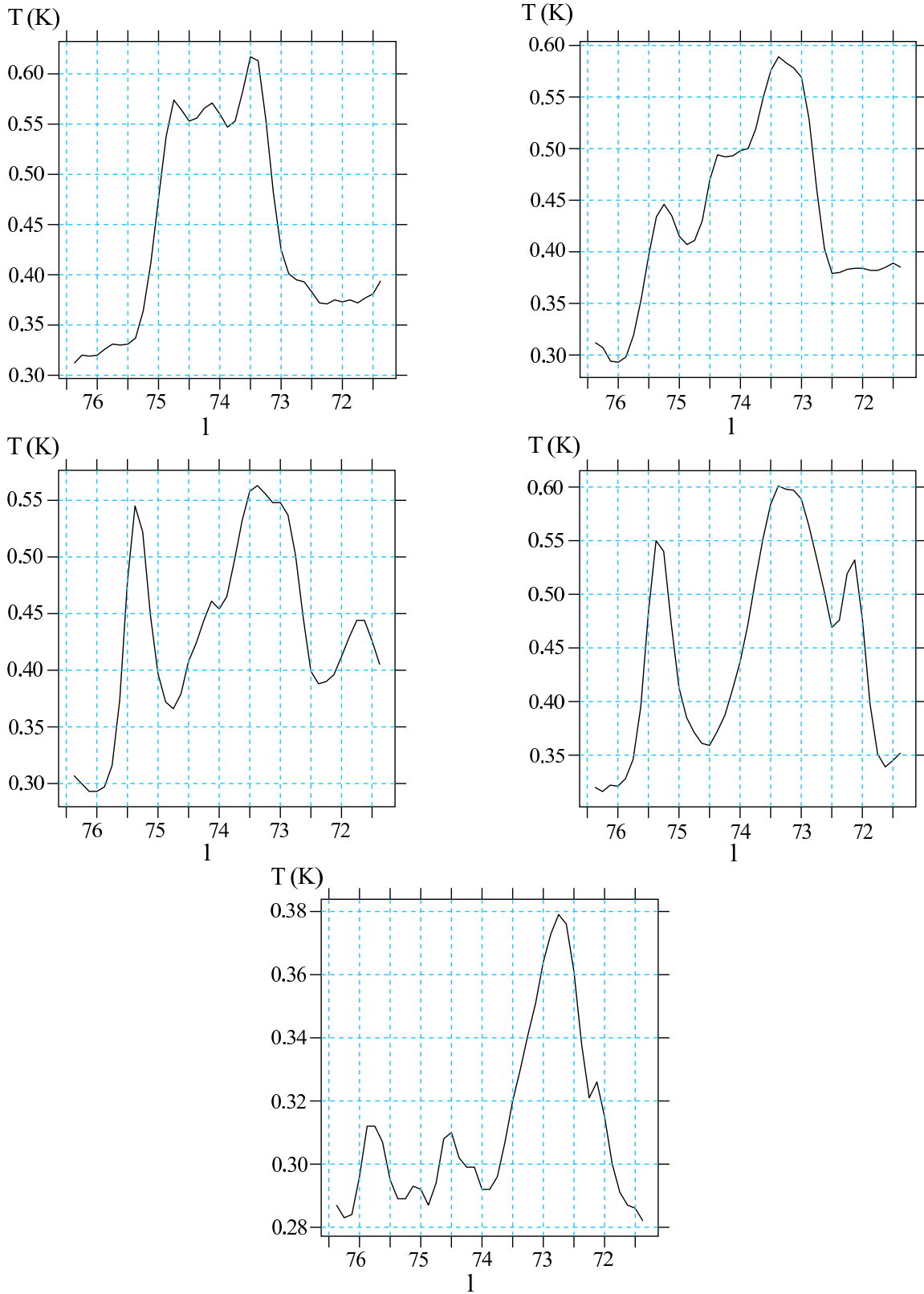


FIG. 6: Temperature profiles at 2720 MHz for Galactic longitude from $76^\circ.5$ to $71^\circ.5$ and for the following values of Galactic latitude: $b = -7^\circ.5$ (top left), $b = -8^\circ$ (top right), $b = -8^\circ.5$ (middle left), $b = -9^\circ$ (middle right) and $b = -10^\circ$ (bottom). Temperatures are given in K, and Galactic longitudes in degrees. Notice that the bottom figure shows the temperature profile at latitude which lies outside (but close enough to) the loop and from that profile we can see what is the highest temperature of the background at $b = -10^\circ$, at 2720 MHz (not of the loop with background).

The mean temperatures and surface brightnesses of this radio loop are computed using data taken from radio-continuum surveys at 2720, 1420, 820, 408 and 34.5 MHz. We have subtracted the background radiation, in order to derive the mean brightness temperature of the SNR alone. First, the temperature of the loop plus background was determined. For every bin in survey we have some value for temperature T_{sum} . We take all bins within the loop border and obtained average temperature $\langle T_{sum} \rangle$ of the loop plus background. Then, the background alone near the loop was estimated. We determine temperature of the background near the outer border of the loop (average value from all data near the outer border of the loop) and that is the background temperature T_{back} . And finally, the difference of these values is calculated to obtain the average temperature of the loop at each frequency: average temperature of the loop is $\langle T_{sum} \rangle - T_{back}$. The areas over which an average brightness temperature is determined at each of the five frequencies are taken to be as similar as possible within the limits of measurement accuracy. T_{min} from Table I means the lower temperature limit between the background and the loop, and T_{max} means the upper temperature limit of the loop. So we used all measured values between T_{min} and T_{max} , inside the corresponding regions of l and b , to calculate the brightness temperature of a loop including the background. The mean brightness temperature for the loop is found by subtracting the mean value of background brightness temperature from the mean value of the brightness temperature over the area of the loop.

After deriving the mean brightness temperatures $T_{b,\nu}$, we have converted these values into surface brightness Σ_ν by:

$$\Sigma_\nu = (2k\nu^2/c^2) T_{b,\nu}, \quad (1)$$

where k is Boltzmann constant and c the speed of light. Results are given in Table I.

III. RESULTS

The radio continuum maps are used for determining the area of the Cygnus loop and for deriving brightness temperatures over it. At each of the five frequencies, the areas are determined to be as similar as possible within the limits of measurement accuracy. There are still some differences between these areas and we think that the major causes of differing borders between the five frequencies are small random and systematic errors in the data. The surface brightnesses of SNRs must be above the sensitivity limit of the observations and must be clearly distinguishable from the Galactic background emission (Green [29]). As it is very difficult to resolve the fainter parts of the loop from the background, they are not taken into account. For evaluation brightness temperatures over the area of the loop we had to take into account background radiation (see Webster [30]). Borders enclosing the spurs

are defined to separate the spur and its background. For the method of calculation see also Borka [25], Borka, Milogradov-Turin, & Urošević [27] and Borka Jovanović & Urošević [28]. As mentioned in these papers, if the value of T_{min} is changed by a small amount, the brightness contours become significantly different. If T_{min} is too small, the area of the spur becomes confused with the background and it becomes obvious that the border has been incorrectly chosen.

The results are given in Tables I, II and III. T_{min} , given in the second column of Table I, is the lower temperature limit, while T_{max} is the upper temperature of the loop and it is also upper temperature limit (because there are no other superposed sources). These temperature limits enable us to distinguish the loop from background. Then we derived the surface brightnesses using equation (1) for each frequency.

The values for brightnesses in $10^{-22} \text{ W}/(\text{m}^2 \text{ Hz Sr})$ can be compared with results for flux densities in Jy. The flux densities can be transformed into brightnesses or vice versa, taking into account that the frequencies have to be the same. Knowing the loop size Ω , the flux densities S_ν given in Jy can be transformed to brightnesses given in $10^{-22} \text{ W}/(\text{m}^2 \text{ Hz Sr})$ by:

$$\Sigma_\nu = S_\nu \times 10^{-26} / \Omega. \quad (2)$$

By use of the spectral indices, the brightnesses can be reduced to 1000 MHz according to relation:

$$\Sigma_{1000} = \Sigma_\nu (1000/\nu)^{(2-\beta)}, \quad (3)$$

where the temperature spectral index $\beta = \alpha + 2$, and α is the spectral index defined by $S_\nu \propto \nu^{-\alpha}$.

Spectrum

The spectrum was generated using mean temperatures at five different frequencies. Best-fit straight line spectrum enables calculation of spectral index as negative value of the line's direction coefficient. In Figure 7 we give spectrum for the three middle frequencies: 1420, 820 and 408 MHz because their spectrum is very well fitted with the straight line (see Figure 7). Frequencies 2720 and 34.5 MHz, lies on very high and on very low ends of the spectrum, as presented in Fig. 8. If for calculation of spectral index we take only three frequencies 1420, 820 and 408 MHz, the result would be $\beta_3 = 2.76 \pm 0.03$. All five frequencies 2720, 1420, 820, 408 and 34.5 MHz, also from linear fit, give $\beta_5 = 2.66 \pm 0.09$. It is steeper spectral index in comparison to average value for Galactic SNRs $\beta = 2.5$ (in Green's catalogue (Green [5]) the adopted value for spectral index is not given because of its variability). Cygnus loop is relatively old SNR. The shock wave has to be weak for evolved SNRs. The steeper spectral indices of SNRs should be expected

TABLE I: Temperatures and brightnesses of Cygnus radio loop at 2720, 1420, 820, 408 and 34.5 MHz

Frequency (MHz)	Temperature limits T_{\min}, T_{\max} (K)	Temperature (K)	Brightness (10^{-22} W/(m ² Hz Sr))
2720	0.395, 0.66	0.160 ± 0.005	3.64 ± 0.12
1420	4.2, 4.9	0.49 ± 0.05	3.04 ± 0.30
820	10.1, 14.0	2.30 ± 0.20	4.75 ± 0.40
408	41, 72	15.3 ± 1.0	7.83 ± 0.50
34.5	34500, 70000	13960 ± 700	50.97 ± 2.56

for the smaller shock wave velocities. Its result obtained from the diffuse particle acceleration theory (Bell [31, 32]). Additionally, Cygnus loop probably expands in low density environment. It looks like large Galactic radio loops - evolved SNRs with the steep spectral indices, immersed in the low density environment (see Borka [25], Borka, Milogradov-Turin, & Urošević [27], and references therein).

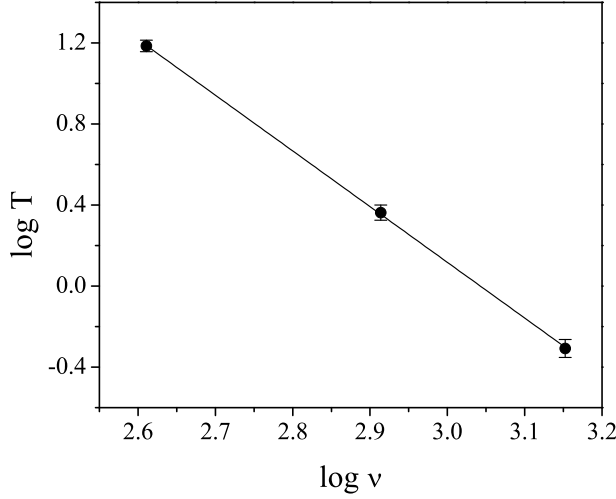


FIG. 7: Cygnus loop spectrum: temperature versus frequency, for three measurements – at 408, 820 and 1420 MHz.

Obtained values $\beta_3 = 2.76 \pm 0.03$ (from three frequencies), $\beta_5 = 2.66 \pm 0.09$ (from all five frequencies), are greater than 2.2 and confirm non-thermal origin of Cygnus loop emission. From Fig. 8 it can be noticed that linear fit is quite satisfactory. The value for the brightness temperature spectral index of the Cygnus loop is rather steep. This is at the high end of the spectral index distribution for SNRs as suggested in Clark & Caswell [33].

$T - T$ plot

The measured data have different resolutions for different frequencies (see §2.1), and therefore in order to obtain $T - T$ plots the data were retabulated so the higher resolution maps are convolved to the resolution of the lowest resolution map. In that way we convolved data at 2720, 1420, 408 and 34.5 MHz to $0''.5 \times 0''.5$

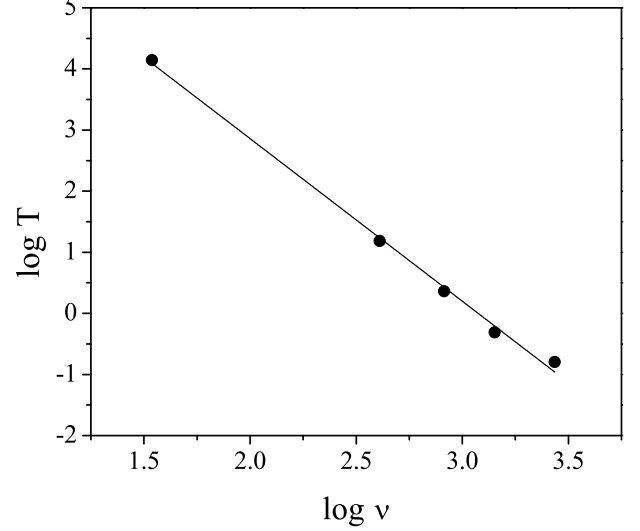


FIG. 8: Cygnus loop spectrum: temperature versus frequency, for five measurements – at 34.5, 408, 820, 1420 and 2720 MHz.

resolution, which is the sampling rate of the 820 MHz survey. These retabulated data are presented in Figure 9 for the following frequencies: 2720 MHz (top left), 1420 MHz (top right), 820 MHz (middle left), 408 MHz (middle right) and 34.5 MHz (bottom). Then, for each frequency pair we used only the common points (with the same (l, b)) which belong to the loop area at both frequencies. In that way we reduced loop area to the same area for different frequencies. The obtained $T - T$ plots for five pairs of frequencies enabled calculating the spectral indices. We calculated two β values for each of these pairs: between 2720–1420, 2720–820, 2720–408, 2720–34.5, 1420–820, 1420–408, 1420–34.5, 820–408, 820–34.5 and 408–34.5 MHz and presented it in Table II. For each of the ten frequency pairs, by interchanging the dependent and independent variables we have obtained two β values for each pair and the mean value of these fit results is adopted as the radio spectral index, as suggested in Uyaniker et al. [11]. Regarding only three frequencies (because their spectrum lies on straight line, see Figure 7) 1420, 820 and 408 MHz, the average value of spectral index from $T - T$ is $\langle \beta_{TT} \rangle_3 = 2.78 \pm 0.41$. Taking into account all five frequencies, we get $\langle \beta_{TT} \rangle_5 = 2.63 \pm 0.30$. It can be noticed that this value agrees well with the corresponding value obtained from spectrum, as expected (see Uyaniker et al. [11]).

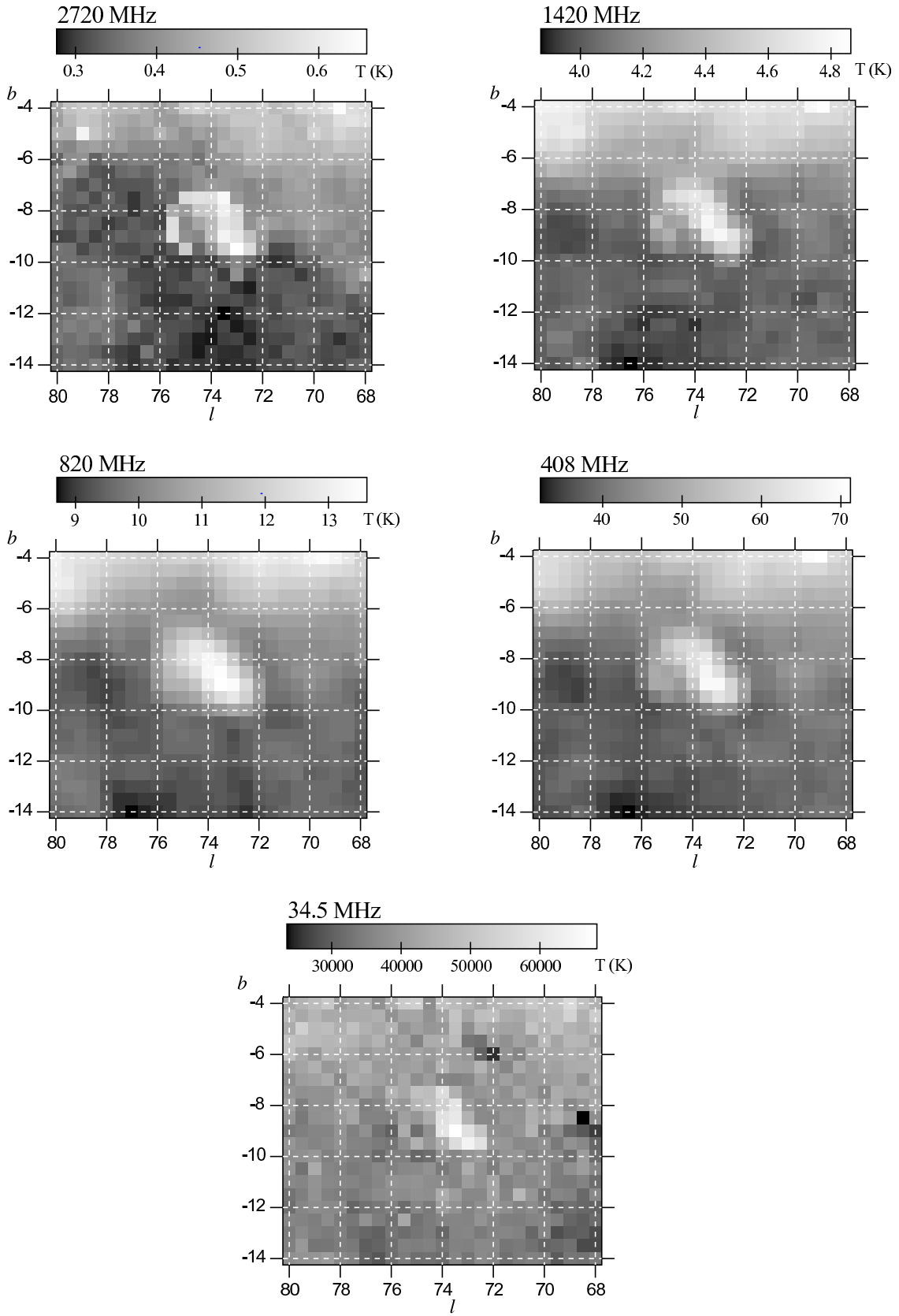


FIG. 9: The data retabulated to $0^\circ.5 \times 0^\circ.5$ resolution, for the following frequencies: 2720 MHz (*top left*), 1420 MHz (*top right*), 820 MHz (*middle left*), 408 MHz (*middle right*) and 34.5 MHz (*bottom*). The HPBW's for these frequencies are $0^\circ.35$, $0^\circ.59$, $1^\circ.2$, $0^\circ.85$ and $0^\circ.7$, respectively. The gray scales of temperatures are given also.

TABLE II: Spectral indices for Cygnus loop from $T - T$ plots, between 2720, 1420, 820, 408 and 34.5 MHz

Frequency (MHz)	2720	1420	820	408	34.5
2720	/	1.52 ± 0.35	1.96 ± 0.53	2.35 ± 0.26	2.57 ± 0.23
1420	2.22 ± 0.76	/	2.27 ± 0.64	2.60 ± 0.28	2.67 ± 0.25
820	2.64 ± 0.61	3.10 ± 0.64	/	2.82 ± 0.31	2.82 ± 0.10
408	2.67 ± 0.26	2.79 ± 0.28	3.10 ± 0.31	/	2.78 ± 0.15
34.5	2.86 ± 0.23	2.95 ± 0.25	2.92 ± 0.10	2.94 ± 0.15	/

Then we calculated mean value of spectral index: regarding spectrum and $T - T$ graphs. Between 1420, 820 and 408 MHz we obtained $\langle \beta \rangle_3 = 2.77 \pm 0.22$, and between 2720, 1420, 820, 408 and 34.5 MHz we obtained $\langle \beta \rangle_5 = 2.64 \pm 0.20$.

IV. DISCUSSION

Spectral index variations with position of more spatial features within the Cygnus loop can be found in paper Leahy [34]. There were studied radio spectral indices by $T - T$ plot method between 2695, 1420 and 408 MHz and found that the bright radio filaments all show negative curvature (steeper at higher frequency), and regions dominated by diffuse emission show positive curvature (flatter at higher frequency).

It can be noticed that mean value of spectral index for Cygnus loop is little higher then the corresponding value obtained from articles (see Uyaniker et al. [11] or Leahy & Roger [26]). Reason for this is different areas used for data of Cygnus loop in these papers. In both papers they used square areas (see page 917 from Uyaniker et al. [11] and page 786 from Leahy & Roger [26]). In these square areas they take into account parts of Cygnus loop and parts of background radiation near Cygnus loop (these parts we do not take into account). We take in account only higher intensity regions from these areas (see Figures 1–5).

TABLE III: Brightness of Cygnus radio loop reduced to 1000 MHz, using spectral index derived in this paper: $\beta_5 = 2.66 \pm 0.09$ (from the spectrum of all five frequencies 2720, 1420, 820, 408 and 34.5 MHz)

Frequency (MHz)	Brightness at 1000 MHz ($10^{-22} \text{ W}/(\text{m}^2 \text{ Hz Sr})$)
2720	7.05 ± 0.86
1420	3.84 ± 0.52
820	4.17 ± 0.29
408	4.33 ± 0.07
34.5	5.52 ± 1.40

In order to compare our values for brightnesses with results for fluxes given in other papers, we transform their calculated fluxes into brightnesses at 1000 MHz. Knowing the loop size Ω we reduce the flux densities given in Jy to brightnesses given in $10^{-22} \text{ W}/(\text{m}^2 \text{ Hz Sr})$ by equation (2) and then by use of the spectral indices, the bright-

nesses are extrapolated to 1000 MHz according to relation (3).

In our previous paper (Borka Jovanović & Urošević [22]) we transformed the flux densities for Cygnus Loop given in Roger et al. [24] at 22 MHz ($S_\nu = 1378 \text{ Jy}$) and Reich, Zhang & Fürst [23] at 863 MHz ($S_\nu = 184 \text{ Jy}$) into Σ_{1000} using loop size $\Omega = 240' \times 170'$ from Reich, Zhang & Fürst [23] and spectral index $\beta = 2.49$ from Trushkin [35]. We obtained that values from (Borka Jovanović & Urošević [22]) agree with previous data. But now in this paper, we use our derived value for spectral index $\beta_5 = 2.66 \pm 0.09$, and obtain even better agreement. From flux densities given in mentioned papers, we calculated the following values for radiation intensities: $\Sigma_{1000} = 3.22 \times 10^{-22} \text{ W}/(\text{m}^2 \text{ Hz Sr})$ from flux given in Roger et al. [24] and $\Sigma_{1000} = 4.84 \times 10^{-22} \text{ W}/(\text{m}^2 \text{ Hz Sr})$ from flux given in Reich, Zhang & Fürst [23].

Using our calculated β_5 and applying relation (3) to our calculated values of Σ_ν at 2720, 1420, 820, 408 and 34.5 MHz, for Σ_{1000} we obtain values given in Table III. Absolute errors for brightnesses at 1000 MHz are calculated in this way: $\Delta \Sigma_{1000} = (\Sigma_{1000}/\Sigma_{\nu 1}) (\Delta \Sigma_{\nu 1} + \Sigma_{\nu 1} \cdot \ln(\nu_1/1000) \cdot \Delta \beta)$, where ν_1 takes values 2720, 1420, 820, 408 and 34.5 MHz.

TABLE IV: The Cygnus loop areas Ω and its angular radii θ at the five frequencies

Frequency (MHz)	$\Omega (^\circ)^2$	$\theta (^\circ)$
2720	7.52	1.547
1420	8.64	1.658
820	9.46	1.735
408	9.88	1.773
34.5	8.44	1.639

Information about variations of brightness and spectrum over radio image is presented by Leahy & Roger [26] and by Uyaniker et al. [9]. The average values reduce the information imprinted in variations of brightness and spectrum over the radio image but give us other interesting information, like explosion energy, surface brightness and distance to the Cygnus radio loop.

With regard to the loop's borders in Figs. 1–5, we derived loop area at each frequency, as well as its corresponding angular radii (see Table IV). An angular radius is obtained in this way: our derived loop area, when approximated with the circle of the same area, gives possibility of determining angular radius as $\theta = \sqrt{\Omega/\pi}$. These areas can be compared to the areas calculated by other authors, e.g. $9(^\circ)^2.80$ at 1420 MHz (Leahy [12])

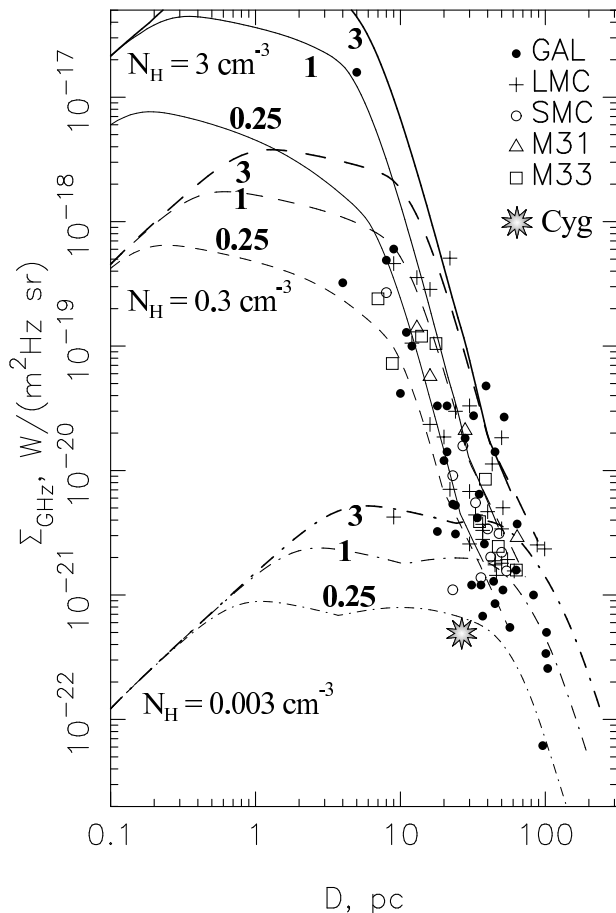


FIG. 10: The surface brightness to diameter diagram from Berezhko & Völk (2004), with value for Cygnus loop added. Three different densities for the interstellar matter (ISM) ($N_H = 3, 0.3$ and 0.003 cm^{-3}) are presented, plus three values for the (SN) explosion energy ($E_{\text{SN}} = 0.25, 1$ and $3 \times 10^{51} \text{ erg}$).

and $11(^{\circ})^{2.33}$ at 863 MHz (Reich, Zhang & Fürst [23]). When their areas are recalculated into angular radii in the way we described, the result are: $1^{\circ}.77$ at 1420 MHz (Leahy [12]) and $1^{\circ}.90$ at 863 MHz (Reich, Zhang & Fürst [23]). It can be noticed that we obtained somewhat smaller values, but it has to be taken into account that other authors estimated only the rectangular map size while we estimated the loop size (inside its contour borders) exactly.

The relation between surface brightness (Σ) and diameter (D) for supernova remnants (SNRs) - so-called the Σ - D relation - is appropriate for description of the radio brightness evolution of these sources. The empirical relations should be used with caution because of the limited usefulness due to selection effects (see Green [5], Urošević et al. [36] and references therein). The updated theoretical relations were derived by Duric & Seaquist [37], based on the Bell's ([31, 32]) diffuse shock particle acceleration theory, and by Berezhko and Völk (Berezhko & Völk [38]) based on the non-linear kinetic theory of the diffuse shock acceleration mechanism. The $\Sigma - D$

diagram at 1 GHz with the theoretically derived evolutionary tracks taken from Berezhko & Völk [38] with our value for the Cygnus loop superposed, is shown in Fig. 10. The $\Sigma - D$ diagram at 1 GHz taken from Berezhko & Völk [38] with the derived value for the Cygnus loop superposed, is shown in Fig. 10. With aim to superpose Cygnus position, we used the following results of our calculations: the mean value of brightnesses at 1 GHz and the diameter, calculated as $D = 2r \sin \bar{\theta}$, where $\bar{\theta} = 1^{\circ}.67$ being mean angular radius for all five frequencies. The distance $r = 0.44 \text{ kpc}$ is taken from Green's catalogue of SNRs (Green [5]). So we added this point to the diagram: $(D, \Sigma) = (25.7 \text{ pc}, 4.98 \times 10^{-22} \text{ W/(m}^2 \text{ Hz Sr)})$. From its position in this diagram it can be concluded that Cygnus loop evolves in the low density environment and the initial energy of supernova (SN) explosion was relatively low (see Fig. 10).

Flux density spectrum

On the basis of values for brightnesses given in the fourth column of Table I and our calculated values for loop size Ω (Table IV), we derived flux values in Jy. The calculated flux densities we give in Table V. As the Cygnus loop is well studied SNR, it is possible to perform a multi-frequency spectral study. In the Fig. 11 we present a summary of some results obtained from other papers and from our study. Our results are labeled with asterisks. So, in this figure, we have seventeen results for the flux density values S_{ν} of Cygnus loop derived in several papers (values are given in Table 3 of Uyaniker et al. [11] and five results from our paper.

It can be seen from Fig. 11 that our added flux values fit very well among other fluxes, which shows correctness of our method, and also that we determined loop area and its brightness well.

TABLE V: Flux densities (Jy) that we calculated at the five frequencies

Frequency (MHz)	Flux density (Jy)
2720	83.37 ± 2.60
1420	80.05 ± 8.13
820	139.35 ± 12.10
408	235.44 ± 15.36
34.5	1309.04 ± 65.65

V. CONCLUSIONS

The main result is method for determination brightness temperature given in article Borka [25] which is developed for large radio loops, and we show that this method is very good for much smaller loop, e.g. Cygnus loop. We check the method by applying it to the Cygnus radio loop at the wide range of frequencies. It is in good agreement with method of $T - T$ graphics and results

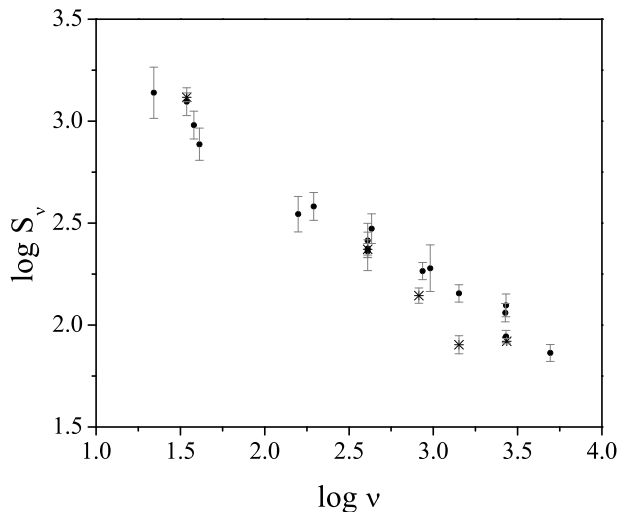


FIG. 11: Spectrum of Cygnus Loop: flux versus frequency for more different frequencies, obtained from all available flux density values (values are given in Table 3 in Uyaniker et al. (2004)) and from values calculated in this paper. We identify our values by asterisks.

obtained with another methods. This method is quite simple because we use brightness temperature isoline to define border of a Cygnus loop. Other authors are using different squared or rectangular areas to determine area of the loop and calculate spectral indices, brightness temperature and the flux density of the loop (Uyaniker et al. [11], page 917 and Leahy & Roger [26], page 786). Also, we calculated flux for Cygnus loop and compare our results with results of other authors in different ranges of frequencies. We show that our results are in good agreement with these results.

We estimated the temperatures and brightness of the Cygnus loop SNR on the basis of observations of the continuum radio emission at the frequencies: 2720, 1420, 820, 408 and 34.5 MHz (this paper and Borka Jovanović & Urošević [22]). The sensitivity of the brightness temperatures are: 5 mK for 2720 MHz, 50 mK for 1420 MHz, 0.2 K for 820 MHz, 1.0 K for 408 MHz and about 700 K T_b for 34.5 MHz. At the frequency of 2720 MHz the

measurements are the most precise (with the least relative errors) so positions of the brightness temperature contours of the loop are the most realistic for this frequency.

Borders between the five frequencies are somewhat different for this SNR probably due to small, random and systematic errors in the calibrated data. Also, we suppose there are uncertainties of about $(2 \times \Delta T)$ 10 mK for 2720 MHz, 100 mK for 1420 MHz, 0.4 K for 820 MHz, 2.0 K for 408 MHz and about 1400 K T_b for 34.5 MHz, in the border due to measurement errors, and there is a tiny difference in the absorption of radio emission in the interstellar medium at different wavelengths (Pacholczyk [39]).

We determined average brightness temperature from a Cygnus radio loop region, after subtraction of a background level. Our obtained values (when all reduced to 1000 MHz for comparison) are in good agreement with the earlier results. We present the radio continuum spectrum of the Cygnus loop using average brightness temperatures at five different frequencies. As it can be seen from Figs. 7 and 8, given linear fit provides reliable spectral index. We present the $T - T$ plots which enable the calculation of spectral index, too.

Also, from our results can be concluded that Cygnus loop evolves in the low density environment and the initial energy of SN explosion was relatively low. This can be read after superposing the position of this loop to theoretical $\Sigma - D$ diagram from Berezhko & Völk [38], which was derived from non-linear kinetic theory of diffuse shock acceleration mechanism.

We showed that method for defining a loop border and for determining the values of temperature and brightness, which we developed for main Galactic loops I-VI, could be applicable to all SNRs.

Acknowledgments

The authors are grateful to the referee whose suggestions substantially improved the paper. This research is supported by the Ministry of Science of the Republic of Serbia through project No. 176005.

-
- [1] McKee, C. F. & Ostriker, J. P. 1977, *ApJ*, 218, 148
 - [2] Salter, C. J. 1983, *Bull. Astron. Soc. India*, 11, 1
 - [3] Green, D. A. 2004, *Bull. Astron. Soc. India*, 32, 335
 - [4] Green, D. A. 2006, *A Catalogue of Galactic Supernova Remnants* (2006 April version), Cavendish Laboratory, Cambridge, UK
 - [5] Green, D. A. 2009, *Bull. Astron. Soc. India*, 37, 45
 - [6] Green, D. A. 1984, *MNRAS*, 211, 433
 - [7] Leahy, D. A., Roger, R. S. & Ballantyne, D. 1997, *AJ*, 114, 2081L
 - [8] Aschenbach, B., & Leahy, D. A. 1999, *A&A*, 341, 602
 - [9] Uyaniker, B., Reich, W., Yar, A., Kothes, R., & Fürst, E. 2002, *A&A*, 389, L61
 - [10] Patnaude, D. J., Fesen, R. A., Raymond, J. C., Levenson, N. A., Graham, J. R., & Wallace, D. J. 2002, *AJ*, 124, 2118
 - [11] Uyaniker, B., Reich, W., Yar, A., & Fürst, E. 2004, *A&A*, 426, 909
 - [12] Leahy, D. A. 2002, *AJ*, 123, 2689
 - [13] Sun, X. H., Reich, W., Han, J. L., Reich, P., & Wielebinski, R. 2006, *A&A*, 447, 937
 - [14] Kundu, M. R. & Becker, R. H. 1972, *AJ*, 77, 459
 - [15] Keen, N. J., Wilson, W. E., Haslam, C. G. T., Graham, D. A. & Thomasson, P. 1973, *A&A*, 28, 197

- [16] Dickel, J. R. & Willis, A. G. 1980, *A&A*, 85, 55
- [17] Reif, K., Reich, W., Steffen, P., Müller, P., & Weiland, H. 1987, *Mitt. Astr. Ges.*, 70, 419
- [18] Reich, P. & Reich, W. 1986 *A&AS*, 63, 205
- [19] Berkhuijsen, E. M. 1972, *A&AS*, 5, 263
- [20] Haslam, C. G. T., Salter, C. J., Stoffel, H., & Wilson, W. E. 1982, *A&AS*, 47, 1
- [21] Dwarakanath, K. S. & Udaya Shankar, N. 1990, *J. Astrophys. Astr.*, 11, 323
- [22] Borka Jovanović, V. & Urošević, D. 2009a, *Publ. Astron. Obs. Belgrade*, 86, 101
- [23] Reich, W., Zhang, X., & Fürst, E. 2003, *A&A*, 408, 961
- [24] Roger, R. S., Costain, C. H., Landecker, T. L., & Swed-lyk, C. M. 1999, *A&AS*, 137, 7
- [25] Borka, V. 2007, *MNRAS*, 376, 634
- [26] Leahy, D. A. & Roger, R. S. 1998, *ApJ*, 505, 784
- [27] Borka, V., Milogradov-Turin, J., & Urošević, D. 2008, *Astron. Nachr.*, 329, 397
- [28] Borka Jovanović, V. & Urošević, D. 2009b, *Astron. Nachr.*, 330, 741
- [29] Green, D. A. 1991, *PASP*, 103, 209
- [30] Webster, A. S. 1974, *MNRAS*, 166, 355
- [31] Bell, A. R. 1978a, *MNRAS*, 182, 147
- [32] Bell, A. R. 1978b, *MNRAS*, 182, 443
- [33] Clark, D. H. & Caswell, J. L. 1976, *MNRAS*, 174, 267
- [34] Leahy, D. A. 1999, *ASP Conferece Series*, 168, 437L
- [35] Trushkin, S. A. 2002, *CATS Database - Astrophysical CATalogs support System, SNRs Spectra Request Form*, http://www.sao.ru/cats/snr_spectra.html
- [36] Urošević, D., Vukotić, B., Arbutina, B., and Sarevska, M. 2010, *ApJ*, 719, 950
- [37] Duric, N., & Seaquist, E. R. 1986, *ApJ*, 301, 308
- [38] Berezhko, E. G., & Völk, H. J. 2004, *A&A* 427, 525
- [39] Pacholczyk, A. G. 1970, *Radio Astrophysics*, Freeman W. H. & Company, San Francisco